JACS
JOURNAL OF THE AMERICAN CHEMICAL SOCIETY
Article
pubs.acs.org/JACS

The Mechanism of E−H (E = N, O) Bond Activation by a Germanium Corrole Complex: A Combined Experimental and Computational Study

Huayi Fang,[†] Huize Jing,[†] Haonan Ge,[†] Penelope J. Brothers,[‡] Xuefeng Fu,*[,†] and Shengfa Ye*[,§]

[†]Beijing National Laboratory for Molecular Sciences, College of Chemistry and Molecular Engineering, Peking University, Beijing 100871, China

[‡]School of Chemical Sciences, University of Auckland, Private Bag 92019, Auckland 1042, New Zealand

[§]Max-Planck Institute for Chemical Energy Conversion, Stiftstraße 34-36, D-45470 Mülheim an der Ruhr, Germany

Supporting Information

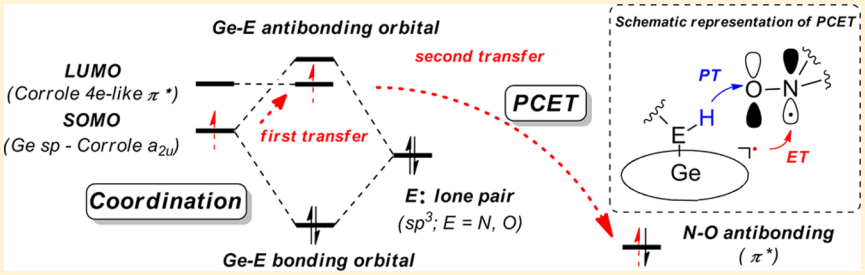

ABSTRACT: (TPFC)Ge(TEMPO) (**1**, TPFC = tris(pentafluorophenyl)corrole, TEMPO$^{\bullet}$ = (2,2,6,6-tetramethylpiperidin-1-yl)oxyl) shows high reactivity toward E−H (E = N, O) bond cleavage in R_1R_2NH (R_1R_2 = HH, ^{n}PrH, ^{i}Pr$_2$, Et$_2$, PhH) and ROH (R = H, CH_3) under visible light irradiation. Electron paramagnetic resonance (EPR) analyses together with the density functional theory (DFT) calculations reveal the E−H bond activation by [(TPFC)Ge]^0(**2**)/TEMPO$^{\bullet}$ radical pair, generated by photocleavage of the labile Ge−O bond in compound **1**, involving two sequential steps: (i) coordination of substrates to [(TPFC)Ge]^0 and (ii) E−H bond cleavage induced by TEMPO$^{\bullet}$ through proton coupled electron transfer (PCET).

INTRODUCTION

Metallo-radical promoted chemical bond activation is receiving intense attention in recent years.[1] Radicaloid routes often occur with lower activation barriers, but are far more rarely encountered due to synthetic difficulties and instability resulting from high reactivity of active radical species. Although a termolecular transition state (TS) was proposed for C−H bond activation by metallo-radical rhodium porphyrins more than 20 years ago,[2] no experimental characterization of the relevant intermediates has been reported yet, and hence, the reaction mechanism remains ambiguous. The growing field of noninnocent ligands has stimulated increasing curiosity for novel electronic structures, intriguing reactivity, and potential application in catalysis.[3] The ligand noninnocence provides an alternate one-electron route for activation of substrates which usually proceeds through two-electron pathways, and emerges as a versatile and effective strategy to enhance the reactivity and selectivity.

Main group elements generally do not undergo the typical transition metal-like elementary processes, such as migration/insertion or oxidation addition/reductive elimination reactions. This is due to the absence of vacant d-orbital coordination sites and the large energy separations among their valence orbitals compared to transition metals which typically possess several energetically accessible frontier orbitals.[4] However, the radicaloid reaction pathway prevails in the chemistry of prototype odd-electron main group species,[5] such as the Gomberg type radicals $R_3E^{\bullet}$ (E = Si, Ge, and Sn) stabilized by a combination of electronic and steric effects.[6] The primary reactions to prepare such radicals, for instance, atom abstraction, oxidation/reduction, or photolysis, are often accompanied by considerable structural rearrangements and undoubtedly result in high reorganization energy which consequently reduce their reactivity. Rational design of precursors is expected to improve both the stability and the reactivity of the corresponding radicals. In this article, the rigid, macrocyclic, aromatic corrole, a trianionic ligand, is used to stabilize Ge(III) which allows us to observe not only the neutral corrole Ge(III) radical ([(TPFC)Ge]^0, **2**),[7] but also the intermediate radical complex in E−H (E = N, O) bond activation. Amine substrates can coordinate to **2** to form an intermediate radical, [(TPFC)Ge(NHR$_1$R$_2$)]^0 (**3**, R_1R_2 = HH, ^{n}PrH, ^{i}Pr$_2$, Et$_2$, PhH), which is verified by EPR spectroscopy. Detailed mechanistic studies on the E−H bond activation indicate that compound **3** undergoes heterolytic N−H bond scission via proton coupled electron

Received: February 2, 2015
Published: May 18, 2015

DOI: 10.1021/jacs.5b01121
J. Am. Chem. Soc. 2015, 137, 7122−7127

transfer (PCET) induced by TEMPO• to yield (TPFC)Ge-(NR_1R_2) (**4**). Following a similar pathway, **2** reacts with water and methanol to quantitatively afford germanium hydroxyl and methoxyl, respectively.

RESULTS AND DISCUSSION

E−H (E = N, O) Bond Activation by Compound 1. (TPFC)Ge(TEMPO) (**1**) reacts efficiently with a series of amine substrates, H_2O and MeOH under visible-light irradiation at ambient temperature to generate **4**, (TPFC)-Ge−OH (**5**), and (TPFC)Ge−OCH_3 (**6**, Supporting Information Figure S1), respectively, in quantitative yields within a few minutes to hours (eq 1, Supporting Information Table S1). The

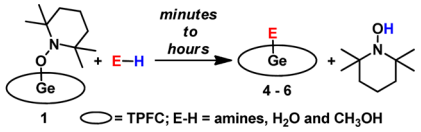

(1)

E−H bond activation by compound **1** can also be performed in the dark, albeit with much lower reaction rates (Supporting Information Table S1), because the photolysis is more efficient in generating active **2**/TEMPO• radical pair than the thermolysis.[7] Interestingly, compound **1** cannot cleave the weaker C−H bonds in CH_4 under similar conditions even at elevated temperatures (E−H bond dissociation energies:[8] H_2O, 118.81 ± 0.07 kcal/mol; MeOH, 105.2 ± 0.7 kcal/mol; NH_3, 107.57 ± 0.06 kcal/mol; CH_4, 105.0 ± 0.1 kcal/mol). Such counterintuitive experimental findings stimulated us to explore the reaction mechanism in order to rationalize this unusual reaction selectivity.

EPR Detection of Amine Coordinated [(TPFC)Ge-($NHEt_2$)]^0 Radical Complexes. In situ photolysis of compound **1** results in the formation of compound **2** and elicits an isotropic singlet (g = 2.0028) at the room-temperature EPR spectrum.[7] Upon addition of excess $NHEt_2$ (400 equiv) to a toluene solution of compound **1** under visible light irradiation, a moderately anisotropic feature appears between the second and third peak of TEMPO• at the low temperature (Figure 1). The observed EPR spectrum qualitatively differs from those of all Ge(III) radicals reported to date,[9] for which no g-anisotropy has been resolved at the X-band frequency.

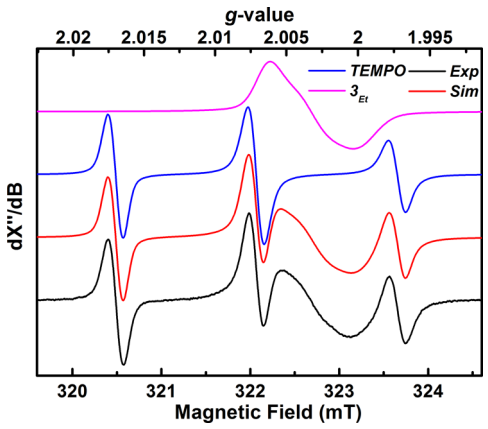

Figure 1. Experimental and simulated EPR spectra of compound **1** with excess $NHEt_2$ under visible light irradiation (1.0 mg of compound **1** and 40 μL of diethylamine in 0.40 mL of toluene, microwave frequency 9.047436 GHz, microwave power 0.4 mW, 158 K).

Moreover, the control experiment indicates that compound **2** cannot be detected under the same conditions (Supporting Information Figure S2). Thus, we tentatively assign this new species to [(TPFC)Ge($NHEt_2$)]^0 ($\mathbf{3}_{Et}$). The B3LYP calculations nicely reproduce the g-values found for $\mathbf{3}_{Et}$ and **2**, and hence confirm this assignment (Table 1), which further lends

Table 1. Comparison of Measured and Calculated g-Values for $\mathbf{3}_{Et}$ and 2

	exp	calcd
$\mathbf{3}_{Et}$, $g_{1,2,3}$	1.9998, 2.0031, 2.0061	1.9991, 2.0035, 2.0042
g_{iso}, Δg	2.0030, 0.0063	2.0023, 0.0051
2, $g_{1,2,3}$	−, −, −	2.0004, 2.0015, 2.0033
g_{iso}, Δg	2.0028, −	2.0017, 0.0029

credence to the proposed electronic structures for both species (vide infra). More importantly, the intensity of the signals of $\mathbf{3}_{Et}$ and TEMPO• decreases synchronously after removing the visible light irradiation (Supporting Information Figure S3), and the ^{1}H NMR spectroscopy shows about 49% of compound **1** is converted to (TPFC)$GeNEt_2$ during the EPR measurement. Therefore, $\mathbf{3}_{Et}$ is a kinetically competent intermediate for the N−H bond scission.

Theoretical Mechanistic Study on E−H Bond Activation. To understand the intriguing reactivity for the E−H bond scission, we perform computational investigations on the reactions of radical pair **2**/TEMPO• with a series of substrates (Figure 2, the computed barriers and reaction free energies for

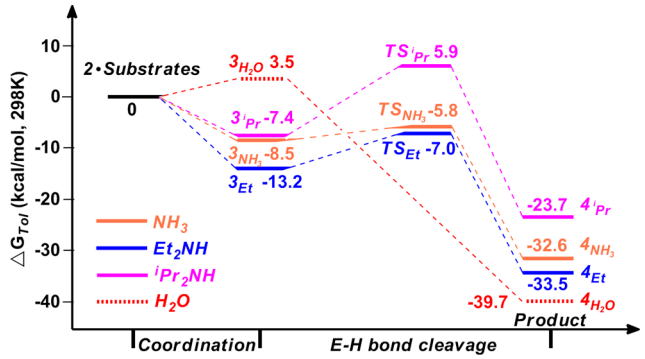

Figure 2. Computed free energy profiles for E−H bond cleavage for NH_3, Et_2NH, $^iPr_2NH$, and H_2O by **2**/TEMPO• radical pair.

all substrates are summarized in Supporting Information Table S2). Hereafter we focus on the mechanism for the N−H bond activation, since it is nearly identical to that for O−H bond scission (Supporting Information Figure S4). Two feasible mechanistic scenarios for N−H bond activation can be envisioned: (i) H atom transfer (HAT) from the N−H moiety to TEMPO• to yield TEMPOH and an aminyl radical which then recombine with **2** to give the final product **4**; (ii) coordination of the amine substrate to **2** to afford a substrate adduct (**3**) as suggested by the above EPR study, followed by N−H bond scission with the assistance of TEMPO•. The direct HAT process can be safely ruled out, because the reactions are computed to strongly endergonic (Supporting Information Tables S5 and S7). By contrast, the formation of **3** is predicted to be exergonic and barrierless for all substrates studied. For the N−H bond cleavage, the reactions with NH_3, $^nPrNH_2$, $NHEt_2$ and $PhNH_2$ are calculated to traverse moderate activation

DOI: 10.1021/jacs.5b01121
J. Am. Chem. Soc. 2015, 137, 7122−7127

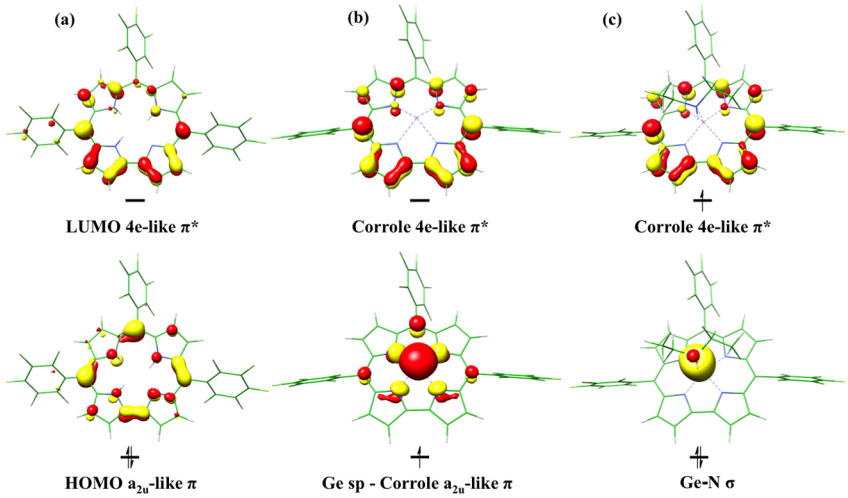

Figure 3. Molecular orbital diagrams for H_3TPFC (a), compounds **2** (b), and $\mathbf{3}_{Et}$ (c),[10] in which quasi-restricted orbitals (QROs)[11] were employed.

barriers (<6.5 kcal/mol), while the reaction with NH^iPr_2 involves a barrier of 13.3 kcal/mol (Supporting Information Table S2). Because the key geometric parameters computed for the TSs (Supporting Information Table S3) are nearly identical for all of the substrates under investigation given the uncertainty of the employed DFT approaches, we attribute the high barrier estimated for NH^iPr_2 to the crowded reaction center in the TS (Supporting Information Figure S5). Remarkably, the computed reaction barriers match the observed reactivity trend reasonably well (for a detail discussion, see the Supporting Information).

Coordination of Amines to [(TPFC)Ge]^0. The experimentally validated B3LYP calculations show the singly occupied molecular orbital (SOMO) of **2** contains significant contributions from the Ge sp-hybridized orbital and the corrole a_{2u}-like orbital[10] (Ge 40%, TPFC 60%) (Figure 3b). Thus, compound **2** is best interpreted as having a resonance electronic structure between Ge(III)($TPFC^{3-}$) and Ge(II)-($TPFC^{2-\bullet}$). By contrast, compound $\mathbf{3}_{Et}$ possesses a Ge(IV) center chelated by a $TPFC^{4-\bullet}$ ligand, indicating the Ge−N_{NHEt_2} σ-bond formation induces an electron transfer from the SOMO of compound **2** into the corrole 4e-like π*-orbital (Figure 3c). Otherwise, one electron would occupy the high-lying Ge−N_{NHEt_2} σ*-antibonding orbital. Moreover, because of electron delocalization, adding an electron in the corrole 4e-like π*-orbital results in negligible structural adjustments of the corrole ligand between compounds **2** and $\mathbf{3}_{Et}$ (Supporting Information Figures S6 and S11). Both factors rationalize the vanishing barriers and the exergonic nature for the substrate binding, despite this process involving the dramatic electronic structure changes.

N−H Bond Cleavage in [(TPFC)Ge(NHR$_1$R$_2$)]^0. For the subsequent N−H bond breaking, in the reactant complex (RC) $TEMPO^\bullet$ is antiferromagnetically coupled to a $TPFC^{4-\bullet}$ radical, thus yielding an overall open-shell singlet ground state (Figure 4a). As $TEMPO^\bullet$ approaches the target N−H bond, the electron originally residing in the corrole π*-orbital gradually shifts into the N−O π* orbital, which results in N−O_{TEMPO} bond lengthening. This electron transfer process culminates in the TS with only marginal unpaired electron density remaining on the corrole ligand (Figure 4b). In the TS, the N−H σ-bond (1.134 Å) in $\mathbf{3}_{Et}$ has not been broken yet, and the N−O bond distance is elongated to 1.366 Å, close to that

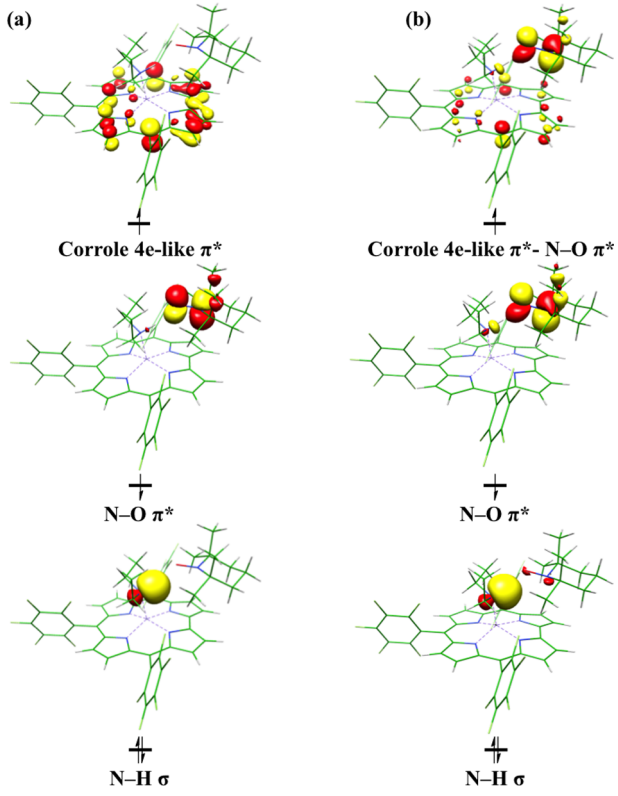

Figure 4. Molecular orbital diagrams for RC (a), and TS_{Et} (b) for the N−H bond cleavage in $\mathbf{3}_{Et}$, in which unrestricted corresponding orbitals (UCOs)[15] and QROs were employed for spin-coupled pair and doubly occupied MOs, respectively.

calculated for $TEMPO^-$ (1.418 Å). After traversing the TS, the $TEMPO^-$-like species accepts a proton from the N−H bond. Taken together, this formal HAT process transforming $TEMPO^\bullet$ to TEMPOH consists of an electron transfer from $TPFC^{4-\bullet}$ and a proton transfer from the substrate, and is therefore best rationalized as a PCET rather than a HAT process, because the electron is transferred separately from the proton.

Typically, it is difficult to unambiguously differentiate HAT and PCET processes,[12] as the product is the same. However, the analysis of the electronic structure changes occurring in

DOI: 10.1021/jacs.5b01121
J. Am. Chem. Soc. 2015, 137, 7122−7127

prototype HAT processes, such as alkane C−H bond activation by organic radicals[13] and high-valent metal−oxo intermediates,[14] revealed that the SOMO, which has the predominant p-orbital character of the abstracting atom (M), directly interacts with the doubly occupied σ-bonding orbital of the cleaving C−H bond, thus leading to a pair of three-center MOs at the TS. The resulting bonding MO becomes doubly occupied and then evolves to the M−H σ-bonding orbital in the product, while the antibonding MO is singly occupied and eventually develops to a C p-orbital of the alkyl radical. However, for the present case, the completely different electronic structure changes have been identified. By reference to the electronic structure of **3**, the preference for PCET lies in the noninnocent character of the corrole ligand. On one hand, the electron implicated in the PCET process is delocalized into the π-system of the TPFC ligand; therefore, the one-electron oxidation of the $TPFC^{4-\bullet}$ ligand only induces marginal geometric distortions (Supporting Information Figures S6−S15) and entails a negligible reorganization energy. On the other hand, the binding of the amine substrate to the Ge(IV) center, a strong Lewis acid, decreases the pK_a value of the N−H motif and hence facilitates the N−H bond heterolysis. Thus, the substrate binding is crucial for the E−H bond activation. Because it is difficult to form a substrate adduct with CH_4, the C−H bond cleavage by radical pair **2**/TEMPO$^\bullet$ cannot easily occur.

For all systems under investigation, we have not succeeded in locating the transition state for the HAT pathway. All attempts aiming to compute the open-shell singlet HAT TS converge back to the corresponding PCET channel, thereby indicating that the HAT trajectory is situated higher in energy. To roughly estimate the HAT barrier, we have explored the reaction of $[(TPFC)Ge(NH_3)]^0$ ($\mathbf{3}_{NH_3}$) and $\mathbf{3}_{Et}$ with TEMPO$^\bullet$ on a triplet state surface, in which the two fragments are *ferromagnetically* coupled. Because the electron transfer from $TPFC^{4-\bullet}$ to TEMPO$^\bullet$ is spin-forbidden, we surmised that with this constraint the HAT pathway would occur. It turns out that the reaction involves a higher barrier (~14−18 kcal/mol) than that found on the open-shell singlet surface, and more importantly also follows a similar PCET mechanism in which the electron originates from the TPFC a_{2u}-like π-orbital (Supporting Information Figures S19 and S21). This result corroborates that the PCET pathway is more energetically favored than the HAT channel, which can be ascribed to the fact that the electron-donating orbital for the HAT pathway, the N−H σ-bonding orbital, lies much lower in energy than the π-orbitals of the noninnocent corrole ligand.

CONCLUDING REMARKS

In conclusion, our combined experimental and theoretical mechanistic study reveals that the activation of the N−H and O−H bonds by radical pair **2**/TEMPO$^\bullet$ proceeds through two sequential steps: (i) coordination of substrates to **2** leading to formation of intermediates **3**, and (ii) E−H bond cleavage by TEMPO$^\bullet$ via PCET. The exergonic coordination of substrates to **2** results in an electron transfer from the SOMO of **2** to the corrole 4e-like π^*-orbital, the SOMO of **3**, which is verified by the EPR detection of $\mathbf{3}_{Et}$ at the low temperature. Then, the electron transfer occurs from the corrole 4e-like π^* orbital to the N−O π^* orbital in TEMPO$^\bullet$, which is coupled with the proton transfer from the E−H bond to the oxygen atom in TEMPO$^\bullet$. The separated transfer of electron and proton is pivotal for the E−H bond scission. The observed reactivity pattern N−H ≈ O−H ≫ C−H can be traced back to their differential coordination ability to afford **3**. In the reaction, the noninnocent corrole ligand features an electron buffer and directs a PCET rather than a HAT pathway for the E−H bond cleavage.

EXPERIMENTAL METHODS

General. All operations were performed using Schlenk techniques under dry argon or nitrogen. Solvents and liquid amines were dried over 4 Å molecular sieves/sodium and degassed prior to use. Water and methanol were degassed prior to use. A 500 W high-pressure xenon lamp (CHF-XM35−500W, Beijing Trustech Co., Ltd.) with a 420−780 nm UV-cutoff filter in the light path was used as the source of visible light. The ^{1}H NMR spectra were recorded on Bruker Avance III 400 and 500 M spectrometer and the given chemical shifts were referenced to the residual protons in the solvent. The single-crystal X-ray diffraction data were collected on a Rigaku MM007HF Saturn724+ diffractometer. The starting material (TPFC)Ge−H and **1** was prepared according to our previously published procedure.[7]

EPR Measurements. The EPR spectra were recorded using JEOL FA-200 spectrometer. Compound **1** (1.0 mg, 9.7×10^{-4} mmol) with diethylamine (40 μL, 400 equiv) was mixed in 0.40 mL of toluene in quartz tube suitable for EPR measurements. The EPR spectrum was recorded at 158 K after a visible light irradiation for 210 min. The program ani_simu developed by JEOL Ltd. was used for spectrum fitting. For the reference EPR measurement, Compound **1** (2.9 mg, 2.8×10^{-3} mmol) was dissolved in 0.40 mL of toluene in quartz tube and the EPR spectrum was recorded at 168 K.

Reactions of Compound 1 with Amines in Dark and under Visible Light Irradiation. Reactions of compound **1** with amines were conducted following the previously reported procedure.[7] Excess amount of amines was added (calcd 3 atm for ammonia gas and 10 equiv for the liquid amines) to a solution of freshly prepared **1** (3.6 mg, 3.5×10^{-3} mmol) in 0.40 mL of deuterated toluene in a J. Young Valve NMR tube. For the reactions in dark, a period of time ranging from 12 h to several days at room temperature or elevated temperatures (up to 110 °C) was needed for the formation of $(TPFC)Ge-NR_1R_2$ (R_1 = H, Et, ^{i}Pr; R_2 = H, ^{n}Pr, ^{i}Pr, Et, Ph; yield, trace to >95%). For the reactions under visible light irradiation, $(TPFC)Ge-NR_1R_2$ (R_1 = H, Et, ^{i}Pr; R_2 = H, ^{n}Pr, ^{i}Pr, Et, Ph) was formed in significant shorter reaction time (15 min to 128 h) with good yields (65% to >95%).

Reactions of Compound 1 with Water and Methanol in Dark. To a solution of freshly prepared **1** (3.6 mg, 3.5×10^{-3} mmol) in 0.40 mL of deuterated toluene in a J. Young Valve NMR tube was added 10 equiv of methanol or water. (TPFC)Ge−OH (**5**) or $(TPFC)Ge-OCH_3$ (**6**) formed quantitatively in dark at room temperature after 300 and 140 min, respectively. The crystal of **6** suitable for X-ray diffraction analysis was obtained by concentration of its methanol solution. (TPFC)Ge−OH (**5**) ^{1}H NMR (400 MHz, C_7D_8) δ(ppm): 9.11 (d, 2H, ^3J(H,H) = 4.0 Hz; β-pyrrole H), 8.89 (d, 2H, ^3J(H,H) = 3.7 Hz; β-pyrrole H), 8.71 (d, 2H, ^3J(H,H) = 3.9 Hz; β-pyrrole H), 8.69 (d, 2H, ^3J(H,H) = 4.3 Hz; β-pyrrole H). $(TPFC)Ge-OCH_3$ (**6**) ^{1}H NMR (400 MHz, C_7D_8) δ(ppm): 9.14 (d, 2H, ^3J(H,H) = 4.1 Hz; β-pyrrole H), 8.90 (d, 2H, ^3J(H,H) = 4.1 Hz; β-pyrrole H), 8.74 (d, 2H, ^3J(H,H) = 4.1 Hz; β-pyrrole H), 8.71 (d, 2H, ^3J(H,H) = 4.2 Hz; β-pyrrole H), −1.13 (s, 3H, OCH_3).

Reactions of Compound 1 with Water and Methanol under Visible Light Irradiation. To a solution of freshly prepared **1** (3.6 mg, 3.5×10^{-3} mmol) in 0.40 mL of toluene-d^8 in a J. Young Valve NMR tube was added 10 equiv of methanol or water. The J. Young Valve NMR tube was placed 0.5 m away from the light source to avoid being heated. The visible light irradiation power is about 18 mW/m^2. Compounds **5** and **6** were formed quantitatively after 85 and 35 min irradiation, respectively.

Computational Setup. All calculations were performed with the ORCA program package.[16] For geometry optimizations, the GGA BP86[17] and hybrid B3LYP[18] density functionals were used in combination with triple-ζ quality def2-TZVP(-f) basis sets[19] for Ge,

DOI: 10.1021/jacs.5b01121
J. Am. Chem. Soc. 2015, 137, 7122−7127

N, O, H and SV(P) basis sets[20] for the remaining elements. The resolution of the identity[21] (RI, for BP86) and RI plus chain of spheres[22] (RIJCOSX, for B3LYP) approximations were used to accelerate the calculations with the auxiliary basis set def2-TZVP/J.[23] We have included the atom-pairwise dispersion correction with Becke-Johnson damping (D3BJ)[24] to account for noncovalent interactions. Solvation effects have been approximately modeled using the conductor-like screening model (COSMO)[25] in the geometry optimizations and the final single point calculations, for which toluene (ε = 2.4) used in experiments was chosen as the solvent. To obtain open-shell singlet solutions of the RCs and TSs for E−H bond cleavage, the broken symmetry formalism[26] has been invoked by using the ORCA key word "brokensym *m*,*n*" (for the present case, $m = n = 1$). The calculation first converges to a triplet solution, in which substrate adduct **3** is ferromagnetically coupled to a TEMPO$^\bullet$ radical, then flipping the spin of the TEMPO$^\bullet$ N−O π^*-orbital generates the initial guess for the self-consistent field (SCF) calculation of the corresponding broken symmetry solution. The nature of the final SCF solution (closed-shell singlet vs open-shell singlet) can be easily differentiated by inspection of the $\langle S^2\rangle$ value or the UCO overlaps.[4b,27] UCOs typically define the magnetic orbitals of the system obtained from broken symmetry calculations. For the present case, a pair of the UCOs, whose overlap is substantially less than 1, represent the TPFC 4e-like π^*- and the TEMPO$^\bullet$ N−O π^*-orbitals. As shown in Supporting Information Tables S4 and S6, the computed $\langle S^2\rangle$ values for all of the RCs and TSs deviated significantly from the ideal value for a closed-shell singlet ($\langle S^2\rangle = 0$), and the estimated UCO overlaps are considerably less than 1. Both observations evidence that our B3LYP and BP86 computations have converged to correct open-shell singlet solutions. All the geometries were fully optimized without symmetry constraints. Harmonic vibrational frequencies were computed to verify the nature of stationary points. All local minima reported in this paper have positive eigenvalues of the Hessian matrix, whereas the TSs have only one negative eigenvalue. Zero-point energies, thermal corrections to 298 K, and entropy terms for the optimized geometries were obtained from the frequency calculations, for which the ideal gas approximation of the standard state (1 atm) is employed. Final single point energies were computed by the B3LYP density functional with the large and flexible def2-TZVPP basis set[19] on all elements. In this paper, we chose the RC in which **3** weakly interacts with TEMPO$^\bullet$ as the reference point to compute the activation barrier. On the basis of our earlier work,[28] for substrate binding in solution choosing the reference point as infinitely separated reactants can lead to an error ~13 kcal/mol for calculated entropy terms. This is due to the fact that only when all species required for an elementary reaction step enter into the same solvent cage can the reaction easily occur; therefore, the changes in the translational entropy for each reactant must be substantially reduced. In fact, a series of pre-equilibriums between reactants have been set up before the actual reaction takes place.[29] Thus, we can reasonably calculate the reaction barrier and free energy with respect to the lowest-energy RC (for the substrate binding, the RC is **2**·substrate in Figure 2 and ***RC_3*** in Supporting Information Tables S4 and S6; for the activation energy barrier evaluation for E−H bond cleavage, the RC is ***RC_4*** in Supporting Information Tables S4 and S6). However, this approximation may slightly underestimate the entropy contributions as the individual translational entropy for each reactant is completely neglected. Because the computed barriers and reaction energies at the BP86-optimized geometries are essentially identical to those calculated at the B3LYP-optimized geometries, in the main text we only discuss the B3LYP results and summarize those based on the BP86 geometries in the Supporting Information.

The EPR parameters were calculated using the B3LYP density functional in combination with the def2-TZVPP basis set for all elements. The structure obtained from the geometry optimization with COSMO[25] was used in the EPR parameter calculations.

■ ASSOCIATED CONTENT

Supporting Information

Detailed discussion of all plausible reaction pathways, Figure S1−S24 and Table S1−S7. The Supporting Information is available free of charge on the ACS Publications website at DOI: 10.1021/jacs.5b01121.

■ AUTHOR INFORMATION

Corresponding Authors

*fuxf@pku.edu.cn

*shengfa.ye@cec.mpg.de

Notes

The authors declare no competing financial interest.

■ ACKNOWLEDGMENTS

We are indebted to Prof. Karl Wieghardt and Dr. Jinshuai Song for fruitful discussions. The work at Peking University was supported by the Natural Science Foundation of China (21171012 and 21322108), and S.Y. gratefully acknowledged financial support from the Max-Planck Society.

■ REFERENCES

(1) (a) Milsmann, C.; Semproni, S. P.; Chirik, P. J. *J. Am. Chem. Soc.* **2014**, *136*, 12099. (b) Fafard, C. M.; Adhikari, D.; Foxman, B. M.; Mindiola, D. J.; Ozerov, O. V. *J. Am. Chem. Soc.* **2007**, *129*, 10318. (c) Napoline, J. W.; Bezpalko, M. W.; Foxman, B. M.; Thomas, C. M. *Chem. Commun.* **2013**, *49*, 4388. (d) Cui, X.; Xu, X.; Jin, L.-M.; Wojtas, L.; Zhang, X. P. *Chem. Sci.* **2015**, *6*, 1219. (e) Paul, N. D.; Mandal, S.; Otte, M.; Cui, X.; Zhang, X. P.; de Bruin, B. *J. Am. Chem. Soc.* **2014**, *136*, 1090. (f) Poli, R. *Angew. Chem., Int. Ed.* **2011**, *50*, 43. (g) Qian, Y. Y.; Li, B. Z.; Chan, K. S. *Organometallics* **2013**, *32*, 1567. (h) Uyeda, C.; Peters, J. C. *Chem. Sci.* **2013**, *4*, 157. (i) Takaoka, A.; Moret, M.-E.; Peters, J. C. *J. Am. Chem. Soc.* **2012**, *134*, 6695. (j) van der Eide, E. F.; Liu, T.; Camaioni, D. M.; Walter, E. D.; Bullock, R. M. *Organometallics* **2012**, *31*, 1775. (k) Puschmann, F. F.; Grützmacher, H.; de Bruin, B. *J. Am. Chem. Soc.* **2010**, *132*, 73.

(2) (a) Wayland, B. B.; Ba, S.; Sherry, A. E. *J. Am. Chem. Soc.* **1991**, *113*, 5305. (b) Sherry, A. E.; Wayland, B. B. *J. Am. Chem. Soc.* **1990**, *112*, 1259.

(3) (a) Lyaskovskyy, V.; de Bruin, B. *ACS Catal.* **2012**, *2*, 270. (b) Gunanathan, C.; Milstein, D. *Acc. Chem. Res.* **2011**, *44*, 588. (c) Thomas, K. E.; Alemayehu, A. B.; Conradie, J.; Beavers, C. M.; Ghosh, A. *Acc. Chem. Res.* **2012**, *45*, 1203. (d) Wang, M.; England, J.; Weyhermüller, T.; Wieghardt, K. *Inorg. Chem.* **2014**, *53*, 2276.

(4) (a) Power, P. P. *Nature* **2010**, *463*, 171. (b) Ye, S.; Geng, C.-Y.; Shaik, S.; Neese, F. *Phys. Chem. Chem. Phys.* **2013**, *15*, 8017.

(5) Woodul, W. D.; Carter, E.; Müller, R.; Richards, A. F.; Stasch, A.; Kaupp, M.; Murphy, D. M.; Driess, M.; Jones, C. *J. Am. Chem. Soc.* **2011**, *133*, 10074.

(6) (a) Power, P. P. *Chem. Rev.* **2003**, *103*, 789. (b) Lee, V. Y.; Sekiguchi, A. *Eur. J. Inorg. Chem.* **2005**, *2005*, 1209.

(7) (a) Fang, H.; Ling, Z.; Lang, K.; Brothers, P. J.; de Bruin, B.; Fu, X. *Chem. Sci.* **2014**, *5*, 916. (b) Fang, H.; Ling, Z.; Brothers, P. J.; Fu, X. *Chem. Commun.* **2011**, *47*, 11677.

(8) Luo, Y.-R. *Comprehensive Handbook of Chemical Bond Energies*; CRC Press: Boca Raton, FL, 2007.

(9) Sheberla, D.; Tumanskii, B.; Bravo-Zhivotovskii, D.; Molev, G.; Molev, V.; Lee, V. Y.; Takanashi, K.; Sekiguchi, A.; Apeloig, Y. *Organometallics* **2010**, *29*, 5596.

(10) The corrole high-lying π-orbitals are labeled according to the symmetry of the corresponding porphyrin orbitals (Figure 3a). (a) Nardis, S.; Paolesse, R.; Licoccia, S.; Fronczek, F. R.; Vicente, M. G.; Shokhireva, T. K.; Cai, S.; Walker, F. A. *Inorg. Chem.* **2005**, *44*, 7030. (b) Ye, S.; Tuttle, T.; Bill, E.; Simkhovich, L.; Gross, Z.; Thiel, W.; Neese, F. *Chem.—Eur. J.* **2008**, *14*, 10839.

(11) Neese, F. *J. Am. Chem. Soc.* **2006**, *128*, 10213.

DOI: 10.1021/jacs.5b01121
J. Am. Chem. Soc. 2015, 137, 7122−7127

(12) (a) Mayer, J. M. *Acc. Chem. Res.* **2011**, *44*, 36. (b) Mayer, J. M. *Acc. Chem. Res.* **1998**, *31*, 441. (c) Dietl, N.; Schlangen, M.; Schwarz, H. *Angew. Chem., Int. Ed.* **2012**, *51*, 5544.
(13) (a) Mayer, J. M.; Hrovat, D. A.; Thomas, J. L.; Borden, W. T. *J. Am. Chem. Soc.* **2002**, *124*, 11142. (b) Li, C.; Danovich, D.; Shaik, S. *Chem. Sci.* **2012**, *3*, 1903. (c) Cembran, A.; Provorse, M. R.; Wang, C.; Wu, W.; Gao, J. *J. Chem. Theory Comput.* **2012**, *8*, 4347.
(14) (a) Ye, S.; Neese, F. *Proc. Natl. Acad. Sci. U.S.A.* **2011**, *108*, 1228. (b) Geng, C.-Y.; Ye, S.; Neese, F. *Angew. Chem., Int. Ed.* **2010**, *49*, 5717. (c) Usharani, D.; Lacy, D. C.; Borovik, A. S.; Shaik, S. *J. Am. Chem. Soc.* **2013**, *135*, 17090.
(15) Neese, F. *J. Phys. Chem. Solids* **2004**, *65*, 781.
(16) Neese, F. *Wiley Interdiscip. Rev.: Comput. Mol. Sci.* **2012**, *2*, 73.
(17) (a) Becke, A. D. *Phys. Rev. A* **1988**, *38*, 3098. (b) Perdew, J. P. *Phys. Rev. B* **1986**, *34*, 7406. (c) Perdew, J. P. *Phys. Rev. B* **1986**, *33*, 8822.
(18) (a) Becke, A. D. *J. Chem. Phys.* **1993**, *98*, 5648. (b) Lee, C.; Yang, W.; Parr, R. G. *Phys. Rev. B* **1988**, *37*, 785. (c) Vosko, S. H.; Wilk, M.; Nusair, M. *Can. J. Phys.* **1980**, *58*, 1200. (d) Stephens, P. J.; Devlin, F. J.; Chabalowski, C. F.; Frisch, M. J. *J. Phys. Chem.* **1994**, *98*, 11623.
(19) Weigend, F.; Ahlrichs, R. *Phys. Chem. Chem. Phys.* **2005**, *7*, 3297.
(20) Schäfer, A.; Horn, H.; Ahlrichs, R. *J. Chem. Phys.* **1992**, *97*, 2571.
(21) (a) Kendall, R. A.; Früchtl, H. A. *Theor. Chem. Acc.* **1997**, *97*, 158. (b) Eichkorn, K.; Weigend, F.; Treutler, O.; Ahlrichs, R. *Theor. Chem. Acc.* **1997**, *97*, 119.
(22) Neese, F.; Wennmohs, F.; Hansen, A.; Becker, U. *Chem. Phys.* **2009**, *356*, 98.
(23) Eichkorn, K.; Treutler, O.; Öhm, H.; Häser, M.; Ahlrichs, R. *Chem. Phys. Lett.* **1995**, *240*, 283.
(24) (a) Grimme, S.; Ehrlich, S.; Goerigk, L. *J. Comput. Chem.* **2011**, *32*, 1456. (b) Grimme, S. *J. Comput. Chem.* **2004**, *25*, 1463. (c) Grimme, S. *J. Comput. Chem.* **2006**, *27*, 1787. (d) Grimme, S.; Antony, J.; Ehrlich, S.; Krieg, H. *J. Chem. Phys.* **2010**, *132*, 154104.
(25) (a) Klamt, A.; Schüürmann, G. *J. Chem. Soc., Perkin Trans. 2* **1993**, 799. (b) Sinnecker, S.; Rajendran, A.; Klamt, A.; Diedenhofen, M.; Neese, F. *J. Phys. Chem. A* **2006**, *110*, 2235.
(26) Noodleman, L. *J. Chem. Phys.* **1981**, *74*, 5737.
(27) (a) Chan, K. S.; Li, X. Z.; Dzik, W. I.; de Bruin, B. *J. Am. Chem. Soc.* **2008**, *130*, 2051. (b) Kirchner, B.; Wennmohs, F.; Ye, S.; Neese, F. *Curr. Opin. Chem. Biol.* **2007**, *11*, 134.
(28) (a) Xue, G.; Geng, C.-Y.; Ye, S.; Fiedler, A. T.; Neese, F.; Que, L., Jr. *Inorg. Chem.* **2013**, *52*, 3976. (b) Ye, S.; Riplinger, C.; Hansen, A.; Krebs, C.; Bollinger, M., Jr.; Neese, F. *Chem.—Eur. J.* **2012**, *18*, 6555. (c) Song, J.; Klein, E. L.; Neese, F.; Ye, S. *Inorg. Chem.* **2014**, *53*, 7500.
(29) Connors, K. A. *Chemical Kinetics: The Study of Reaction Rates in Solution*; VCH: New York, 1990; pp 99−101.

DOI: 10.1021/jacs.5b01121
J. Am. Chem. Soc. 2015, 137, 7122−7127